Sustainable Energy & Fuels
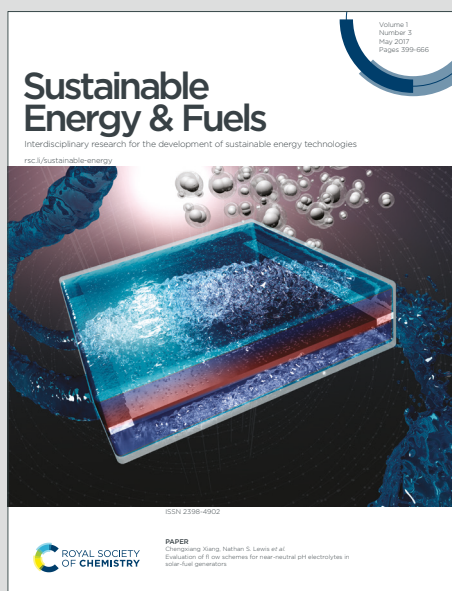
Interdisciplinary research for the development of sustainable energy technologies

Accepted Manuscript

Volume 1
Number 3
May 2017
Pages 399-666

Sustainable
Energy & Fuels

Interdisciplinary research for the development of sustainable energy technologies

rsc.li/sustainable-energy

ISSN 2398-4902

ROYAL SOCIETY
OF CHEMISTRY

PAPER
Chengxiang Xiang, Nathan S. Lewis et al.
Evaluation of fl ow schemes for near-neutral pH electrolytes in
solar-fuel generators

ROYAL SOCIETY
OF CHEMISTRY

rsc.li/sustainable-energy

Journal Name

ARTICLE

Pt atoms on doped carbon nanosheets with ultrahigh N content as a superior bifunctional catalyst for hydrogen evolution/oxidation

Zhen Zhang [a, b], Cheng Jiang [b], Ping Li [c], Qi Feng [b], Zhiliang Zhao [b], Keguang Yao [b], Jiantao Fan [b], Hui Li [b] *, Haijiang Wang [d]

Pt single-atom catalysts (SACs) have shown great potential for electrochemical catalysis. However, no systematic study of their bifunctional catalysis for the hydrogen evolution reaction (HER) and the hydrogen oxidation reaction (HOR) has yet been published. More significantly, the reported catalytic capabilities of Pt SACs have almost been exclusively measured using a rotating disk electrode (RDE) with a three-electrode configuration, which does not accurately reflect the catalysts' performance during operation within single-cell devices. Herein, we demonstrate the immobilization of isolated Pt atoms on a carbon nanosheet support doped with ultrahigh N content (12.1 at%; Pt/NCS) to create a bifunctional HER/HOR catalyst. Compared with commercial Pt/C, the developed Pt/NCS catalyst delivered high utilization as well as excellent mass activity enhancement and stability for both reactions. As a final test, the rigorous catalyst evaluation was conducted in both a proton exchange membrane (PEM) electrolyzer and a PEM fuel cell. As expected, with only half the Pt loading of commercial Pt/C, Pt/NCS-based electrodes in the electrolyzer and the fuel cell still exhibited slightly better performance than those based on Pt/C. This work constitutes a huge step from the academic study of Pt-based SCAs to their industrial application, and it should focus more attention on the harsh evaluation and optimization of SACs within commercial-scale devices.

1. Introduction

Hydrogen's uniqueness as an energy carrier makes it one of the most promising alternatives for replacing traditional fossil fuels, due to its high energy density, cleanness, and sustainability.[1, 2] The hydrogen evolution reaction (HER) and hydrogen oxidation reaction (HOR) are two of the key process that play significant roles in a hydrogen economy. The HER is the cathode reaction of water electrolysis to generate hydrogen gas, and the HOR is the anode reaction of fuel cell that converts hydrogen to electricity in an environmentally friendly way.[3-6] As a pair of inverse reactions, the HER and HOR can be assembled with a proton exchange membrane (PEM) to construct electrochemical hydrogen pump devices that can realize hydrogen compression and storage.[7, 8] To date, noble metal catalysts have seemed indispensable to achieve sufficiently

high kinetic activity for the HER/HOR; however, the metals' scarcity and consequent high cost hinder their widespread commercialization.[9-11] Hence, it is essential to overcome the challenges of developing inexpensive alternatives. Although impressive results based on non-noble metal electrocatalysts have been achieved, nothing can, as yet, replace commercial Pt/C, especially in terms of its remarkable HOR activity. Tremendous effort has been put into synthesizing Pt-based alloys or core-shell architectures,[12-14] aiming to decrease overall Pt usage. Unfortunately, these catalysts usually require complicated synthesis procedures, casting a shadow over the possibility of their large-scale production.

Very recently, single-atom catalysts (SACs) have drawn substantial attention because their architecture holds the promise of maximum atomic utilization efficiency, high mass activity, and catalytic selectivity.[15-17] Many SACs prepared by various synthetic methods have been widely used in various electrochemical catalysis, such as oxygen reduction reaction (ORR), oxygen evolution reaction (OER), carbon dioxide reduction reaction(CO$_2$RR), and nitrogen reduction reaction (NRR).[18-21] Benefiting from atomic metal centers with nearly zero Gibbs free energy for hydrogen absorption, Pt-based SACs are playing an increasingly significant role in HER/HOR electrocatalysis. With respect to the HER, Pt SACs have been developing rapidly. Sun and co-workers reported the preparation of isolated Pt atoms and clusters immobilized on N-doped graphene through atomic layer deposition technology.[22] Based on experimental characterizations and theoretical

a School of Materials Science and Engineering, Harbin Institute of Technology, Harbin, 150001, China
b Department of Materials Science and Engineering, Southern University of Science and Technology, Shenzhen, 518055, China
c Center for Spintronics and Quantum Systems, State Key Laboratory for Mechanical Behavior of Materials, School of Materials Science and Engineering, Xi'an Jiaotong University, Xi'an, 710049, China
d Department of Mechanical and Energy Engineering, Southern University of Science and Technology, Shenzhen, 518055, China
* Prof. H. Li (E-mail: hui.li@sustech.edu.cn)
Electronic Supplementary Information (ESI) available: Calculation details for Tafel fitting, C_{dl}, and mass activity. Computation methods and models for ΔE_{H^*}. Comparison table with reported catalytic activity. See DOI: 10.1039/x0xx00000x

ARTICLE

calculations, the authors found that the excellent HER activity originated from the partially unoccupied states of the Pt 5d orbitals.

Yet despite such very encouraging progress, we are still a long way from achieving the commercialization of SACs for the HER. First of all, research focusing on the rational design of coordination environments for SACs is still in its infancy. Furthermore, easily accessible and cost-effective synthesis strategies for larger throughput have not been developed. Last, but most important, the excellent HER activities for Pt SACs in previous reports were almost exclusively obtained using a rotating disk electrode (RDE) with a three-electrode configuration, leading to overly optimistic results that suggest Pt SACs could completely surpass and replace commercial Pt/C. But what if this exciting HER activity could also be realized in a rigorous PEM electrolyzer cell? This has rarely been proposed but should be investigated.

In contrast to the HER, much less attention has been focused on SAC-based HOR catalysts due to the historic fact that Pt loading at the anode used to contribute only 20% of the total Pt loading in PEM fuel cells, the majority being required for the comparatively sluggish cathode ORR. But with the tremendous progress achieved over the past decade on ORR catalysts and catalyst layer design, cathode Pt loading has dropped greatly from ~ 0.4 to ~ 0.15 mg_{Pt} cm^{-2}, rendering the contribution at the anode significant.[23-25] The U.S. Department of Energy's target of 0.125 mg cm^{-2} total Pt loading to achieve the large-scale commercialization of fuel cells is ever to be met, hence reducing Pt loading at the anode is essential.[26] In addition, during the frequent startup and shutdown of a fuel cell, oxygen reduction inevitably occurs around Pt particles on the anode side, causing irreversible degradation.[27, 28] The conventional and currently industrial method is to add IrO_2 catalyst to promote oxygen evolution reaction (ORR) and then inhibit the carbon corrosion process.[29, 30] But the addition of expensive ORR catalyst further enhances the cost. Fortunately, Pt SACs endowed with ORR-suppressing selectivity,[31] are likely to cut off the reversal voltage circuit at the initial ORR step at the anode, making them a promising option as HOR catalysts. To date, however, there has been very little relevant research.

In light of all these factors, we herein report an atomically dispersed Pt catalyst immobilized on carbon nanosheets doped with ultrahigh N content (Pt/NCS). RDE measurements indicated the Pt/NCS catalyst had excellent HER performance with low overpotential (18.1 mV at a current density of 10 mA cm^{-2}), high mass activity (10.22 A mg_{Pt}^{-1} at 50 mV), and better stability than commercial Pt/C. High Pt utilization, excellent enhancement of mass activity, and ORR-suppressing selectivity were also achieved for the HOR. In addition, we explored the catalytic mechanism for the HER/HOR using density functional theory (DFT) calculations. Most significantly, as well as verifying the catalyst's high intrinsic activity through RDE, we performed membrane-electrode assembly (MEA) measurements using Pt/NCS as the cathode for a PEM electrolyzer, and as the anode in a PEM fuel cell. Despite ultralow Pt loading (half of the Pt/C reference catalyst's loading), the Pt/NCS-based electrolyzer and fuel cell exhibited somewhat better current density and power density than those based on Pt/C. This work not only has investigated the bifunctional HER/HOR activity of a Pt SAC

but also has made progress towards industrial applications for hydrogen production and fuel cells.

2. Results and discussion

2.1 Synthesis and characterization of electrocatalyst

The synthesis process for Pt/NCS is illustrated in Fig. 1a. First, C_3N_4-derived NCS was prepared according to a previous report[32], with some modifications (see details in the experimental section). The melamine was thermally condensed to form layered C_3N_4 at the initial low-temperature annealing. Subsequently, D-glucosamine hydrochloride formed carbon skeleton cross-linking with C_3N_4 structure. Via the following high-temperature pyrolysis, C_3N_4 was completely decomposed to supply N species, thus leading to the formation of graphene-like carbon nanosheets with high content N-doping. Then, the as-prepared NCS was used as a support to absorb the Pt precursor by wet impregnation. Finally, after drying, the product was re-dissolved in ethylene glycol and then treated with microwave irradiation, after which the absorbed $PtCl_4^{2-}$ ions turned into atomically dispersed Pt sites. Scanning electron microscopy (SEM) (Fig. 1b, c) and transmission electron microscopy (TEM) (Fig. 1d) revealed the graphene-like nanosheet morphology of Pt/NCS, which was basically the same as that of pure NCS (Fig. S1). The prepared Pt/NCS was further characterized by atomic-resolution aberration-corrected high-angle annular dark-field scanning TEM (HAADF-STEM) to directly observe the characteristics of the Pt species on the NCS. In Fig. 1e, numerous individual bright spots can be seen, confirming the existence of isolated Pt atoms. Additional HAADF-STEM images from different sections are provided in Fig. S2; these too show no clusters or particles. Elemental mapping (Fig. 1f-i) showed the uniform, dense dispersions of N and Pt atoms. No metallic Pt diffraction peaks were observed in the X-ray diffraction (XRD) patterns (Fig. 2a), once again indicating the absence of large Pt nanoparticles.

Fig. 1 Fabrication and structural characterization of Pt/NCS. (a) Schematic illustration of
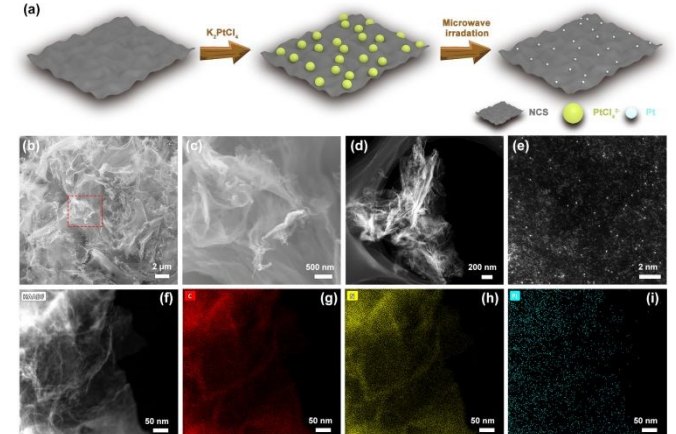
synthesis procedure. (b, c) SEM images. (d) TEM image. (f) Atomic-resolution HAADF-STEM image. (f-i) HAADF image and corresponding EDX elemental mapping of C, N, and Pt.

It is generally acknowledged that the support plays several essential roles in the preparation of SACs: absorbing the metal precursor, preventing aggregation, and immobilizing the metal atoms. Undeniably, carbon-based materials are preferable. To improve the loading of metal atoms, a support should have the following features: high specific surface area,[33, 34] abundant pores,[35] plentiful carbon defects,[36, 37] and rich heteroatoms, such as nitrogen and oxygen.[38-40] As shown in Fig. 2b, after the atomic Pt species were trapped, the Raman results indicated a slight decrease in the I_D/I_G value, implying the anchoring of Pt atoms on carbon defect sites.[39] As calculated from the N_2 sorption isotherms (Fig. 2c) using the BET and BJH models, the NCS support exhibited a high specific surface area of 586.9 $m^2\ g^{-1}$, a total pore volume of 1.4 $cm^3\ g^{-1}$, and a mean pore diameter of 9.2 nm. The high porosity ensured sufficient contact with the reactants (humidified H_2 gas or water molecules) during operation, which also enabled rapid mass transport through the catalyst layer in a single-cell device, especially under high current density conditions.
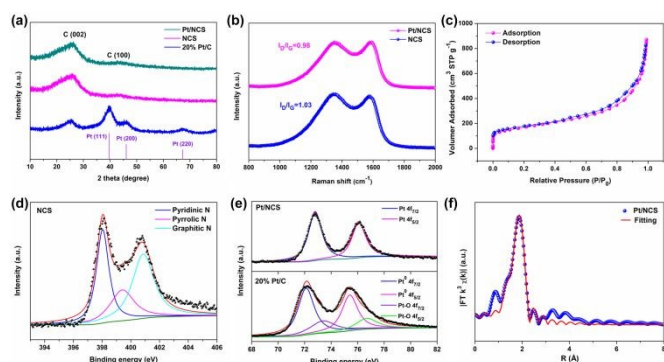

Fig. 2 XRD patterns of Pt/NCS, NCS support, and commercial 20% Pt/C. (b) Raman spectra of Pt/NCS and NCS. (c) N_2 sorption isotherms of NCS. (d) High-resolution N1s XPS spectra of NCS. (e) Pt 4f patterns of Pt/NCS and commercial 20% Pt/C. (f) Fourier transform of EXAFS R-space fitting curves for Pt/NCS.

We carried out X-ray photoelectron spectroscopy (XPS) measurements to identify the chemical compositions of the NCS, Pt/NCS, and commercial Pt/C samples; the results are shown in Fig. S3. The survey plot of the prepared Pt/NCS clearly indicated the presence of elemental N and Pt. The high-resolution N1s pattern of the pure NCS carbon support is plotted in Fig. 2d. The signals with binding energies of 398.0, 399.4, and 400.9 eV correspond to pyridinic, pyrrolic, and graphitic N dopants, respectively. It is well known that N heteroatoms are of great importance in building a coordination environment to immobilize Pt single atoms. Generally, the reported N content in final carbon products is low, but surprisingly, the total N content in the NCS support reached 12.1 at%. This abundance of N dopants favored the anchoring of single Pt atoms and helped prevent aggregation.

The results of inductively coupled plasma-mass spectroscopy (ICP-MS) indicated the atomic Pt content reached 1.4 wt%. With respect to the Pt 4f patterns (Fig. 2e) as compared with those of metallic Pt in commercial 20% Pt/C, which had binding energies of 72.2 and 75.5 eV, Pt/NCS showed a positive shift to 72.7 eV for Pt 4f7/2 and to 76.0 eV for Pt 4f5/2, implying the configuration of Pt-N bonds. To investigate the local atomic and electronic structures, extended X-ray absorption fine structure (EXAFS) spectroscopy was

carried out, and the Fourier transform (FT) fitting results are provided in Fig. 2f and Table S1. As expected, no characteristic peak around 2.5 Å (corresponding to the Pt-Pt bond[39]) was detected, indicating the absence of metallic Pt particles. Notably, a dominant peak was located at 1.89 Å, which corresponded to Pt-N bonds, further confirming that isolated Pt atoms were stably immobilized by neighboring N heteroatoms.[33, 35] It can therefore be concluded that we successfully fabricated atomic Pt species on a carbon nanosheet support with high doped N content.

2.2 Electrochemical performance towards HER/HOR with RDE testing

We systematically investigated the bifunctional performance toward the HER and HOR of the Pt/NCS catalyst and commercial 20% Pt/C. First, the intrinsic activity was evaluated in a standard three-electrode electrochemical cell with RDE. Solutions of 0.5 M H_2SO_4 and 0.1 M $HClO_4$ were used as media for the HER and HOR measurements, respectively. All the results were corrected with iR compensation, using an R value based on the electrochemical impedance spectroscopy (EIS) results in Fig. S4. As shown in Fig. 3a, the NCS support made no contribution to HER performance. However, after the anchoring of single Pt atoms, the activity was notably enhanced. Specifically, Pt/NCS required small overpotentials of 18.1 and 89.1 mV to drive current densities of 10 and 100 mA cm^{-2}, respectively, values slightly better than those of commercial 20% Pt/C (27.4 and 93.9 mV). More importantly, after normalization of the current density with Pt loading, Pt/NCS demonstrated an ultrahigh mass activity of 10.22 A mg_{Pt}^{-1} at an overpotential of −50 mV, which was much larger than that of 20% Pt/C (1.49 A mg_{Pt}^{-1}). This result demonstrated that the atomic Pt sites possessed much higher Pt utilization efficiency than the Pt particles, resulting in impressive improvement in the HER activity. It is also worth mentioning that for the HER, Pt/NCS outperformed many other previously reported Pt-based catalysts (Table S2). In addition, as can be seen in Fig. 3b, Pt/NCS had a Tafel slope of 30 mV dec^{-1}, very close to that of 20% Pt/C, implying that the HER process followed the Volmer-Tafel route, and the electrochemical desorption of hydrogen was the rate-determining step.
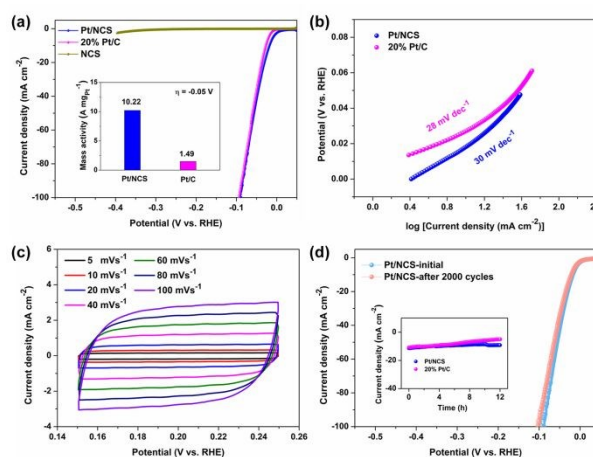

Fig. 3 (a) HER linear sweep voltammetry (LSV) curves of Pt/NCS, NCS, and commercial 20% Pt/C at a scan rate of 5 mV s^{-1} in 0.5 M H_2SO_4 solution; inset is the mass activity at −0.05 V. (b) Tafel plots of Pt/NCS and 20% Pt/C. (c) CV curves of Pt/NCS at different scan rates from 5 to 100 mV s^{-1}. (d) LSV curves of Pt/NCS before and after 2000 CV

cycles; inset are *i-t* stability test results for Pt/NCS and 20% Pt/C, run at constant potentials to drive an initial current density of 10 mA cm⁻².

It is generally accepted that in an acidic electrolyte, the electrochemical active surface area (ECSA) is proportional to the electrical double-layer capacitance (C_{dl}).[41, 42] Based on the cyclic voltammetry (CV) results at different scan rates (Fig. 3c), the C_{dl} of Pt/NCS was fitted to 27.3 mF cm⁻² (Fig. S5), markedly higher than that of the NCS support (Fig. S6), which can be attributed to the presence of isolated Pt atoms. To assess durability, we carried out a continuous potential cycling test. As shown in Fig. 3d, negligible decay was observed when the LSV curves before and after 2000 cycles were compared, indicating the robust stability of Pt/NCS. After a long-term *i-t* test (12 h), the Pt/NCS catalyst also displayed better stability than commercial 20% Pt/C (inset Fig. 3d). The XRD and high-resolution Pt 4f patterns Pt/NCS after stability testing were provided in Fig. S7. No Pt particles related peaks was observed in XRD and the XPS result still presented positive shift compared with commercial Pt/C. The above experimental results verified the outstanding catalytic activity of Pt/NCS towards the HER.
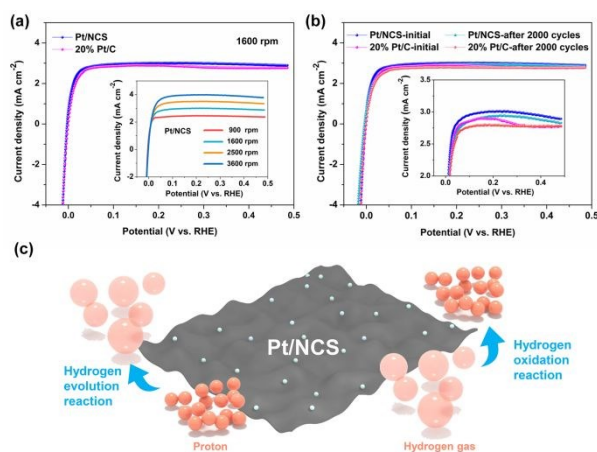

Fig. 4 (a) Polarization curves of Pt/NCS and commercial 20% Pt/C in H₂-saturated 0.1 M HClO₄ at a scan rate of 10 mV s⁻¹ and a rotation rate of 1600 rpm; inset are polarization curves of Pt/NCS at a scan rate of 10 mV s⁻¹ for various rotation rates (b) Polarization curves of Pt/NCS and commercial 20% Pt/C as HOR catalysts in the first cycle and after 2000 cycles; inset shows enlargement of the limiting current density region. (c) Schematic illustration of Pt/NCS bifunctional catalysis towards HER/HOR.

We investigated the HOR activity of the as-prepared Pt catalyst in an acidic (0.1 M HClO₄) solution. Fig. 4a displays the polarization curves obtained in a H₂-saturated solution at a rotation rate of 1600 rpm. As expected, the Pt/NCS catalyst with ultralow Pt loading exhibited HOR performance similar to that of commercial 20% Pt/C. The onset overpotential of the HOR on the Pt/NCS electrode was observed to be about zero, implying its high intrinsic activity to drive the HOR process. We also obtained the polarization curves at different electrode rotation rates (inset Fig. 4a). The limiting current density increased gradually as the rotation speed increased. According to the Koutecky-Levich equation, current density is proportional to the square root of rotation rate;[43, 44] details are provided in Supporting Information. After linear fitting (Fig. S8), Pt/NCS exhibited a mass activity of 2.04 A mg$_{Pt}$⁻¹ at a potential of 0.05 V, greatly outperforming 20% Pt/C (0.31 A mg$_{Pt}$⁻¹). The stability of Pt/NCS for the HOR was measured via continuous CV tests in a

H₂-saturated solution at 1600 rpm; the negligible loss of current density suggested good stability (Fig. 4b). Generally, commercial Pt anode catalysts are active for both the HOR and the ORR. Hence, during the startup/shutdown of fuel cell vehicles, oxygen in the anode channel can cause undesirable oxygen reduction at the anode, leading to irreversible degradation. Fortunately, as shown in Fig. S9, Pt/NCS strongly suppressed ORR activity. Its combination of high HOR activity, good stability, and ORR-suppressing selectivity thus make Pt/NCS a promising candidate for the fuel cell anode catalyst.

On the basis of these results we can conclude that this Pt/NCS catalyst possesses unique bifunctional HER/HOR activity; that is, it can efficiently catalyze the transitions between protons and hydrogen gas, as illustrated in Fig. 4c. Its superb HER/HOR mass activity benefits from high utilization of Pt atoms and sufficient active sites. When it comes to theorizing on the origin of active sites, the hydrogen binding energy (ΔE_{H*}) is acknowledged to be essential for describing the hydrogen reaction, and the values of ΔE_{H*} close to that of Pt is what researchers are consistently pursuing.[45, 46] To shed light on the catalytic mechanism, we conducted density functional theory (DFT) calculations to obtain the value of ΔE_{H*}. According to the EXAFS fitting results, the coordination number of Pt-N was about 2. We therefore constructed several configurations (Fig. S10) in which Pt bonded with two N atoms. Pt/NCS catalyst exhibits ΔE_{H*} values of −0.39 eV (Ⅰ) and −0.35 eV (Ⅱ), very close to that of Pt (111) (−0.4 eV),[47] suggesting a favorable adsorption of H and excellent HER and HOR activity.

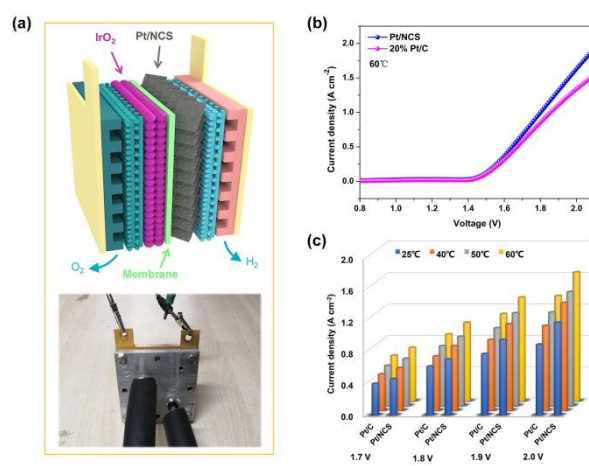## 2.3 MEA measurements with a PEM electrolyzer and a PEM fuel cell

Fig. 5 (a) Schematic illustration and photo of the PEM electrolyzer device. (b) Polarization curves measured at 60°C using Pt/NCS and 20% Pt/C as cathode catalyst. (c) Comparison of current density for Pt/NCS and 20% Pt/C, recorded for different voltages at various temperatures.

Although high HER/HOR activity was achieved with a RDE, in terms of practical application, it was necessary to further examine the catalyst's performance in a PEM electrolyzer and a fuel cell device, due to significant gap between RDE and MEA tests.[48] Specifically, compared to the thin-film RDE technique, in which the activity is dominated by kinetics, MEA performance in a single cell is

Journal Name

determined not only by intrinsic kinetics but also by mass transport of the reactants and products (protons, electrons, gases, and water); hence, evaluating the catalytic ability using a MEA in a single cell is the final benchmark.[49, 50] First, we assembled a PEM electrolyzer using Pt/NCS as the cathode and commercial IrO_2 as the anode. A detailed schematic diagram of the components and a photograph of the PEM electrolyzer are shown in Fig. 5a. Fig. S11 also presents the prepared catalyst coated membrane (CCM), showing the cathode layer's porosity, which was beneficial for fast mass transport during cell operation. For comparison, commercial 20% Pt/C was used as the cathode with a Pt loading of 0.050 mg cm^{-2}, twice that of Pt/NCS. As anticipated, despite the relatively lower Pt loading, the Pt/NCS-based PEM electrolyzer exhibited better performance than 20% Pt/C (Fig. 5b), with high current densities of 1.00 and 1.90 A cm^{-2} for 1.8 and 2.1 V at 60°C. We also evaluated the performance of Pt/NCS-based and 20% Pt/C-based electrolyzers at different temperatures, the results of which are provided in Fig. S12 and Fig. 5c, showing that higher temperature yielded higher electrolytic activity. All the above results definitively confirmed the superiority of Pt/NCS compared to 20% Pt/C.
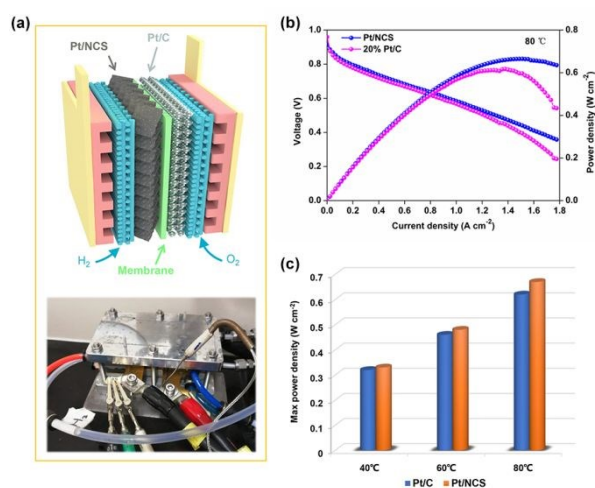

Fig. 6. (a) Schematic illustration and photo of PEM fuel cell device. (b) Polarization curves measured at 80°C using Pt/NCS and 20% Pt/C as anode catalyst. (c) Comparison of maximum power density for Pt/NCS and 20% Pt/C at various temperatures.

For fuel cell measurement, we also assembled a MEA using Pt/NCS as the anode catalyst to drive the HOR process. Our homemade fuel cell device is shown in Fig. 6a. A CCM was fabricated using Pt/NCS (0.025 mg_Pt cm^{-2}) and 47% Pt/C (0.033 mg_Pt cm^{-2}) as the anode and cathode, respectively (Fig. S13). Note that the cathode loading was purposely designed to allow sufficient ORR activity at the cathode, ensuring that the anode HOR was the main rate-determining step for the whole fuel cell. A CCM using commercial 20% Pt/C (0.050 mg_Pt cm^{-2}) was also prepared as the reference sample. Fig. 6b presents the relationship between current density, voltage, and power density. With only half of the Pt loading compared to 20% Pt/C, the Pt/NCS-based fuel cell still delivered a power density of 0.58 W cm^{-2} at a current density of 1.0 A cm^{-2}, which was nearly equivalent to that of 20% Pt/C. In addition, Pt/NCS exhibited a maximum power density of 0.67 W cm^{-2} at 1.51 A cm^{-2}, slightly higher than that of Pt/C (0.62 W cm^{-2}). The actual

fuel cell performance at different temperatures was also measured, and the results are presented in Fig. 6c and Fig. S14.

Overall, this Pt/NCS catalyst containing abundant and uniformly dispersed Pt atoms immobilized on a carbon nanosheet support showed enormous potential for low-cost, efficient fuel cell application. It should be noted that within a three-electrode testing system, Pt/NCS with a loading just one-seventh that of 20% Pt/C on a RDE yielded similar HER and HOR activity; however, when it came to MEA testing, the Pt loading had to be increased to approximately one half that of 20% Pt/C to achieve the same performance. This is largely because the thin-film RDE technique operates at relatively small current densities, and the influence of mass transport is minor. In other words, kinetic activity dominates the electrode's behavior. But the working conditions in a MEA are much harsher; along with intrinsic activity, mass transport across the entire catalyst layer also matters, especially during operation under high current densities. Hence, the thickness of the anode Pt/NCS catalyst layer was thicker than that of 20% Pt/C (Fig. S15), enlarging the reactant/product transfer pathway. Ionomer content and distribution are also essential factors when it comes to SACs, and these areas require long-term, in-depth exploration. To sum up, we believe that catalytic performance at the MEA level has not yet been completely realized. In our laboratory, further extensive research is underway, focused on translating SACs into highly active catalyst layers with superior performance through mass transfer enhancement and ionomer tuning.

3. Conclusions

In summary, we have demonstrated an atomically dispersed Pt catalyst supported on NCS that is highly active towards both the HER and the HOR. This Pt/NCS has many advantages: (1) its high doped N content (12.1 at%) favors the immobilization of sufficient isolated Pt atoms; (2) the NCS support possesses a large specific surface area and high porosity, allowing efficient contact with the electrolyte and fast mass transport; and (3) the unique coordination environment endows the Pt atoms with appropriate hydrogen binding energy. Hence, the developed Pt/NCS catalyst exhibits greatly enhanced mass activity and excellent stability compared to commercial 20% Pt/C. Further, with only half the Pt loading of commercial Pt/C, similar or even slightly higher performance was realized within a Pt/NCS-assembled PEM electrolyzer and fuel cell.

This work is a huge step toward the practical application of Pt SACs in low-cost, efficient hydrogen production and fuel cells. We anticipate that rigorous MEA measurement and characterization within whole devices will increasingly be included in the early development of SACs, because it is very helpful, indeed essential, for their commercialization.

Experimental

Chemicals

D-glucosamine hydrochloride (GAH), melamine, potassium tetrachloroplatinate (K_2PtCl_4), isopropyl alcohol (IPA), and ethylene glycol were purchased from Aladdin Industrial Corp. Sulfuric acid (H_2SO_4), perchloric acid ($HClO_4$), and methanol were obtained from

Shanghai Chemical Reagents. Platinum on graphitized carbon (20 wt% Pt/C) catalyst was purchased from Johnson Matthey. The proton exchange membrane in this work was Gore M820.15. The carbon papers were purchased from Achates International Trading Co., Ltd. All of the chemicals used in this experiment were of analytical grade and used without further purification. Deionized water (18.25 MΩ) was used for all the experiments.

Synthetic procedures

10 g of melamine and 0.5 g of GAH were dissolved in 50 mL water/methanol (v:v, 1:9) solution. Then the mixed solution was sonicated for 0.5 h and subjected to magnetic stirring at 60°C. After evaporation, the solid mixture was ground into powder and then transferred into a crucible. The sample was heated under an argon atmosphere to 600°C at a rate of $2°C\ min^{-1}$ and kept at 600°C for 1 h to form C_3N_4. Subsequently, the C_3N_4 was carbonized to form NCS by further heat treatment at 800°C for 6 h. It was then washed with 0.5 M H_2SO_4 once, followed by rinsing with deionized water. Finally, the NCS was obtained by lyophilization overnight.

In a typical synthesis, 50 mg of NCS was dispersed with 50 mL deionized water and sonicated for 1 h. K_2PtCl_4 aqueous solution (5 mg mL^{-1}, 1 mL) was added dropwise into the NCS solution. After 0.5 h of sonication, the mixed solution was kept under magnetic stirring for 6 h at room temperature. The resulting solution was then filtered and washed with deionized water several times, and dried at 50°C under vacuum. The product was re-dissolved in 20 mL ethylene glycol, stirred for 1 h, and subjected to microwave irradiation treatment for 10 s. After cooling to room temperature, the sample was washed with deionized water several times and dried at 50°C under vacuum overnight to obtain the Pt/NCS catalyst.

Characterizations

The morphology of the catalyst was investigated using a TESCAN field emission scanning electron microscope (SEM). Transmission electron microscopy (TEM), high-resolution transmission electron microscopy (HRTEM), high-angle annular dark field scanning transmission electron microscopy (HAADF-STEM), and X-ray energy dispersive spectroscopy (EDS) mapping were conducted using a double Cs-corrector FEI Titan Themis G2. Powder X-ray diffraction (XRD) was performed on a Bruker AXS D8-Focus with Cu Kα radiation (γ = 1.54056 Å). X-ray photoelectron spectroscopy (XPS) measurements were taken with a PHI 5000 Versa Probe III. Inductively coupled plasma (ICP) measurement was performed on an Agilent Technologies 7700 series instrument. The specific surface area was calculated from nitrogen adsorption-desorption isotherms collected at 77 K on a Micromeritics ASAP 2020 physisorption instrument. The Pt L3-edge extended X-ray absorption structure (EXAFS) spectroscopy of the as-prepared sample was acquired at the beamline BL01C1.

Three-electrode electrochemical measurements

Electrochemical measurements were initially carried out on a Solartron electrochemical workstation, equipped with a Compact Pine Rotator system. A typical three-electrode configuration at room temperature was constructed, where a glassy carbon rotating disk electrode (RDE) with a diameter of 5 mm (disk geometric area =

0.196 cm²), a reversible hydrogen electrode, and a graphite rod functioned as the working electrode, reference electrode, and counter electrode, respectively. Solutions of 0.5 M H_2SO_4 and 0.1 M $HClO_4$ were used as media for the HER and HOR measurements, respectively. To prepare the working electrode, 4 mg of Pt/NCS catalyst and 50 μL Nafion solution (5 wt%) was dispersed in 1 mL water/ethanol (v:v, 1:4) solution. After sonication for 1 h, the catalyst ink (15 μL) was then dropped onto the RDE, giving a catalyst loading of 0.292 mg cm^{-2} (4.08 $μg_{Pt}\ cm^{-2}$). For HER measurements, linear sweep voltammetry (LSV) was recorded at room temperature in N_2-saturated 0.5 M H_2SO_4 using a scan rate of 5 mV s^{-1} and a rotation rate of 1600 rpm. Electrochemical impedance spectroscopy (EIS) was conducted in the frequency range of 0.1–10,000 Hz. The polarization curves were all corrected using the *iR*-compensation that was determined from the EIS experiments. For the durability test, 2000 CV cycles were performed in the potential range of 0.05 to −0.15 V vs. RHE at a scan rate of 50 mV s^{-1}. In addition, a long-term stability test was carried out using the i-t curves (12 h) for Pt/NCS and commercial 20% Pt/C at a constant potential that yielded an initial current density of 10 mA cm^{-2}.

The HOR measurements were carried out in 0.1 M $HClO_4$ aqueous solutions. After the electrolyte was purged with pure hydrogen for at least 0.5 h, HOR polarization curves were obtained by sweeping the potential from −0.05 to 0.50 V at a scan rate of 10 mV s^{-1} under different rotation rates (900, 1600, 2500, and 3600 rpm). Stability was measured during 2000 CV cycles in the potential range from −0.05 to 0.20 V at a scan rate of 50 mV s^{-1}. During the stability test, H_2 gas was continuously pumped into the solution, and the RDE rotation rate was fixed at 1600 rpm.

Proton exchange membrane (PEM) electrolyzer and fuel cell testing

PEM electrolyzer measurements were performed to further evaluate the catalyst's activity and verify the industrial practicability of Pt/NCS catalysts towards electrochemical hydrogen production. The membrane electrode assembly (MEA) and PEM electrolyzer were prepared as follows: First, the membrane underwent a four-step immersion in (i) 5 wt% H_2O_2 solution, (ii) deionized water, (iii) 0.5 M H_2SO_4 solution, and (iv) deionized water at 80°C; each step lasted 40 min. Second, to prepare the anode, 75 mg of commercial IrO_2 and 230 mg Nafion (10 wt%) were mixed with 1 mL of water and 4 mL of IPA. After 1 h of sonication, the catalyst ink was blade-coated onto a polytetrafluoroethylene (PTFE) sheet, yielding an anode catalyst loading of 2.5 $mg_{IrO2}\ cm^{-2}$. To prepare the cathode, 20 mg Pt/NCS catalyst and 200 mg Nafion (10 wt%) were mixed with 0.5 mL of water and 3.5 mL of IPA. The ink was sprayed onto the membrane until a loading of 0.025 $mg_{Pt}\ cm^{-2}$ was reached. For comparison, commercial 20% Pt/C was also used as a cathode, with a loading of 0.050 $mg_{Pt}\ cm^{-2}$. Subsequently, the catalyst coated membranes were prepared by transferring the anode layer to the other side of the membrane via a hot-pressing process at 130°C using a pressure 30 kg cm^{-2} for 1 min. Then the MEA was fabricated by placing the CCM between the anode and cathode gas diffusion layers (GDLs). Finally, the as-prepared MEA was assembled with two flow-field plates, fluorinated ethylene propylene gaskets, and stainless steel end plates, using a torque of 6.0 N. During testing,

Journal Name

ARTICLE

deionized water was pre-heated to the required temperature and then continuously pumped into the anode of the homemade PEM electrolyzer device. The polarization curves were recorded from 0.6 to 2.1 V.

For the PEM fuel cell evaluation, Pt/NCS was use as the anode catalyst to drive the HOR process. The ink preparation was similar to what is described above. The ink was sprayed onto the membrane to achieve a loading of 0.025 mg_{Pt} cm^{-2}. For comparison, an anode using commercial Pt/C was prepared with a loading of 0.050 mg_{Pt} cm^{-2}. For the cathode, a catalyst ink using 47 wt% commercial Pt/C was blade-coated onto a PTFE sheet to achieve a loading of 0.33 mg_{Pt} cm^{-2}. The cathode Pt loading was purposely higher than required, so as to drive the cathode ORR at a sufficiently high reaction rate that the anode HOR was the main rate-determining process. Then a CCM with an area of 4.5 cm^2 was fabricated via hot-pressing at 165°C and a pressure of 70 psi. A structural representation and a photograph of the homemade fuel cell device are shown in Fig. 6a. Finally, the fuel cell measurements were performed with a fuel cell test station (Shanghai Hephas Energy Corporation), with pure H_2 and air fed into the anode and cathode, respectively. The cell temperature was fixed at 40, 60 and 80°C, respectively, by heated circulating water, and a relative humidity (RH) of 100% was maintained with bubbling humidifiers. The gas stoichiometry value was 1.3 for H_2 and 2.0 for air, with the same back pressure of 0.1 MPa at the anode and cathode sides.

Conflicts of interest

There are no conflicts to declare.

ORCID

Zhen Zhang: 0000-0003-4095-0206
Ping Li: 0000-0001-8285-8921
Hui Li: 0000-0001-8356-6154

Acknowledgements

Notes and references

1. S. Chandrasekaran, L. Yao, L. Deng, C. Bowen, Y. Zhang, S. Chen, Z. Lin, F. Peng and P. Zhang, *Chemical Society Reviews*, 2019, **48**, 4178-4280.
2. I. Staffell, D. Scamman, A. Velazquez Abad, P. Balcombe, P. E. Dodds, P. Ekins, N. Shah and K. R. Ward, *Energy & Environmental Science*, 2019, **12**, 463-491.
3. Z. Chen, X. Duan, W. Wei, S. Wang and B.-J. Ni, *Journal of Materials Chemistry A*, 2019, **7**, 14971-15005.
4. Y. Cong, I. T. McCrum, X. Gao, Y. Lv, S. Miao, Z. Shao, B. Yi, H. Yu, M. J. Janik and Y. Song, *Journal of Materials Chemistry A*, 2019, **7**, 3161-3169.
5. J. Zhu, L. Hu, P. Zhao, L. Y. S. Lee and K.-Y. Wong, *Chemical Reviews*, 2020, **120**, 851-918.
6. E. S. Davydova, S. Mukerjee, F. Jaouen and D. R. Dekel, *ACS Catalysis*, 2018, **8**, 6665-6690.
7. M. Lee and X. Huang, *Electrochemistry Communications*, 2020, **117**, 106777.
8. C. Jackson, L. F. J. M. Raymakers, M. J. J. Mulder and A. R. J. Kucernak, *Journal of Power Sources*, 2020, **472**, 228476.
9. S. Lu and Z. Zhuang, *Science China Materials*, 2016, **59**, 217-238.
10. T. Wang, H. Xie, M. Chen, A. D'Aloia, J. Cho, G. Wu and Q. Li, *Nano Energy*, 2017, **42**, 69-89.
11. G. Huang, W. Liang, Y. Wu, J. Li, Y. Q. Jin, H. Zeng, H. Zhang, F. Xie, J. Chen, N. Wang, Y. Jin and H. Meng, *Journal of Catalysis*, 2020, **390**, 23-29.
12. S. T. Hunt, M. Milina, Z. Wang and Y. Román-Leshkov, *Energy & Environmental Science*, 2016, **9**, 3290-3301.
13. Y. Liu, S. Liu, Z. Che, S. Zhao, X. Sheng, M. Han and J. Bao, *Journal of Materials Chemistry A*, 2016, **4**, 16690-16697.
14. K. Elbert, J. Hu, Z. Ma, Y. Zhang, G. Chen, W. An, P. Liu, H. S. Isaacs, R. R. Adzic and J. X. Wang, *ACS Catalysis*, 2015, **5**, 6764-6772.
15. Y. Zhu, J. Sokolowski, X. Song, Y. He, Y. Mei and G. Wu, *Advanced Energy Materials*, 2020, **10**, 1902844.
16. Q. Hu, G. Li, X. Huang, Z. Wang, H. Yang, Q. Zhang, J. Liu and C. He, *Journal of Materials Chemistry A*, 2019, **7**, 19531-19538.
17. Z. W. Chen, L. X. Chen, C. C. Yang and Q. Jiang, *Journal of Materials Chemistry A*, 2019, **7**, 3492-3515.
18. L. Bai, Z. Duan, X. Wen, R. Si, Q. Zhang and J. Guan, *ACS Catalysis*, 2019, **9**, 9897-9904.
19. Q. Zhang, Z. Duan, Y. Wang, L. Li, B. Nan and J. Guan, *Journal of Materials Chemistry A*, 2020, **8**, 19665-19673.
20. Q. Zhang and J. Guan, *Journal of Power Sources*, 2020, **471**, 228446.
21. Q. Zhang and J. Guan, *Advanced Functional Materials*, 2020, **30**, 2000768.
22. N. Cheng, S. Stambula, D. Wang, M. N. Banis, J. Liu, A. Riese, B. Xiao, R. Li, T. K. Sham, L. M. Liu, G. A. Botton and X. Sun, *Nat Commun*, 2016, **7**, 13638.
23. S. Sui, X. Wang, X. Zhou, Y. Su, S. Riffat and C.-j. Liu, *Journal of Materials Chemistry A*, 2017, **5**, 1808-1825.
24. G. Wang, L. Zou, Q. Huang, Z. Zou and H. Yang, *Journal of Materials Chemistry A*, 2019, **7**, 9447-9477.
25. Y.-J. Wang, N. Zhao, B. Fang, H. Li, X. T. Bi and H. Wang, *Chemical Reviews*, 2015, **115**, 3433-3467.
26. V. Yarlagadda, M. K. Carpenter, T. E. Moylan, R. S. Kukreja, R. Koestner, W. Gu, L. Thompson and A. Kongkanand, *ACS Energy Letters*, 2018, **3**, 618-621.
27. S. W. Yun, S. A. Park, T. J. Kim, J. H. Kim, G. W. Pak and Y. T. Kim, *ChemSusChem*, 2017, **10**, 489-493.
28. B. Genorio, R. Subbaraman, D. Strmcnik, D. Tripkovic, V. R. Stamenkovic and N. M. Markovic, *Angew Chem Int Ed Engl*, 2011, **50**, 5468-5472.
29. L. Hu, B. K. Hong, J.-G. Oh and S. Litster, *ACS Applied Energy Materials*, 2019, **2**, 7152-7161.
30. T. Joo, L. Hu, B. K. Hong, J.-G. Oh and S. Litster, *Journal of Power Sources*, 2020, **472**, 228439.
31. L. Zhang, K. Doyle-Davis and X. Sun, *Energy &*

Environmental Science, 2019, **12**, 492-517.

32.   J. Wang, Z. Wei, S. Mao, H. Li and Y. Wang, *Energy & Environmental Science*, 2018, **11**, 800-806.

33.   T. Li, J. Liu, Y. Song and F. Wang, *ACS Catalysis*, 2018, **8**, 8450-8458.

34.   K. Chi, Z. Chen, F. Xiao, W. Guo, W. Xi, J. Liu, H. Yan, Z. Zhang, J. Xiao, J. Liu, J. Luo, S. Wang and K. P. Loh, *Journal of Materials Chemistry A*, 2019, **7**, 15575-15579.

35.   Z. Zhang, Y. Chen, L. Zhou, C. Chen, Z. Han, B. Zhang, Q. Wu, L. Yang, L. Du, Y. Bu, P. Wang, X. Wang, H. Yang and Z. Hu, *Nat Commun*, 2019, **10**, 1657.

36.   Q. Cheng, C. Hu, G. Wang, Z. Zou, H. Yang and L. Dai, *J Am Chem Soc*, 2020, **142**, 5594-5601.

37.   X. Bao, Y. Gong, Y. Chen, H. Zhang, Z. Wang, S. Mao, L. Xie, Z. Jiang and Y. Wang, *Journal of Materials Chemistry A*, 2019, **7**, 15364-15370.

38.   S. Ye, F. Luo, Q. Zhang, P. Zhang, T. Xu, Q. Wang, D. He, L. Guo, Y. Zhang, C. He, X. Ouyang, M. Gu, J. Liu and X. Sun, *Energy & Environmental Science*, 2019, **12**, 1000-1007.

39.   J. Ji, Y. Zhang, L. Tang, C. Liu, X. Gao, M. Sun, J. Zheng, M. Ling, C. Liang and Z. Lin, *Nano Energy*, 2019, **63**, 103849.

40.   K. Huang, R. Wang, H. Wu, H. Wang, X. He, H. Wei, S. Wang, R. Zhang, M. Lei, W. Guo, B. Ge and H. Wu, *Journal of Materials Chemistry A*, 2019, **7**, 25779-25784.

41.   Y. Guan, Y. Feng, J. Wan, X. Yang, L. Fang, X. Gu, R. Liu, Z. Huang, J. Li, J. Luo, C. Li and Y. Wang, *Small*, 2018, **14**, e1800697.

42.   H. Zhang, P. An, W. Zhou, B. Y. Guan, P. Zhang, J. Dong and X. W. Lou, *Science Advances*, 2018, **4**, eaao6657.

43.   M. K. Kundu, R. Mishra, T. Bhowmik and S. Barman, *Journal of Materials Chemistry A*, 2018, **6**, 23531-23541.

44.   Y. Li, J. Abbott, Y. Sun, J. Sun, Y. Du, X. Han, G. Wu and P. Xu, *Applied Catalysis B: Environmental*, 2019, **258**, 117952.

45.   K. Ojha, S. Saha, P. Dagar and A. K. Ganguli, *Physical Chemistry Chemical Physics*, 2018, **20**, 6777-6799.

46.   H. Wang, W. Fu, X. Yang, Z. Huang, J. Li, H. Zhang and Y. Wang, *Journal of Materials Chemistry A*, 2020, **8**, 6926-6956.

47.   Y. Yang, X. Sun, G. Han, X. Liu, X. Zhang, Y. Sun, M. Zhang, Z. Cao and Y. Sun, *Angew Chem Int Ed Engl*, 2019, **58**, 10644-10649.

48.   L. Pan, S. Ott, F. Dionigi and P. Strasser, *Current Opinion in Electrochemistry*, 2019, **18**, 61-71.

49.   D. Banham and S. Ye, *ACS Energy Letters*, 2017, **2**, 629-638.

50.   A. Kongkanand and M. F. Mathias, *J Phys Chem Lett*, 2016, **7**, 1127-1137.

Sustainable Energy & Fuels Accepted Manuscript

Isolated Pt atoms on N-doped carbon nanosheets exhibit excellent bifunctional catalytic performance towards

hydrogen evolution/oxidation reaction (HER/HOR).